Published in final edited form as:
Environ Sci Technol. 2014 January 21; 48(2): 1166–1174. doi:10.1021/es403929b.

Zirconium-carbon hybrid sorbent for removal of fluoride from water: oxalic acid mediated Zr(IV) assembly and adsorption mechanism

Velazquez-Jimenez Litza Halla[a], **H Hurt Robert**[b], **Matos Juan**[c], and **Rangel-Mendez Jose Rene**[a]

[a]Division of Environmental Sciences, Instituto Potosino de Investigación Científica y Tecnológica, A.C., Camino a la Presa San José 2055, Col. Lomas 4[a] sección, C.P. 78216, San Luis Potosí, S.L.P., México

[b]School of Engineering/Institute for Molecular and Nanoscale Innovation (IMNI), Brown University, Providence, Rhode Island, 02912, United States

[c]Department of Photocatalysis and Alternative Energies, Venezuelan Institute for Scientific Research (IVIC), 20632, Caracas 1020-A, Venezuela

Abstract

When activated carbon (AC) is modified with zirconium(IV) by impregnation or precipitation, the fluoride adsorption capacity is typically improved. There is significant potential to improve these hybrid sorbent by controlling the impregnation conditions, which determine the assembly and dispersion of the Zr phases on carbon surfaces.

Here, commercial activated carbon was modified with Zr(IV) together with oxalic acid (OA) used to maximize the zirconium dispersion and enhance fluoride adsorption. Adsorption experiments were carried out at pH 7 and 25 °C with a fluoride concentration of 40 mg L^{-1}. The OA/Zr ratio was varied to determine the optimal conditions for subsequent fluoride adsorption. The data was analyzed using the Langmuir and Freundlich isotherm models. FTIR, XPS and the surface charge distribution were performed to elucidate the adsorption mechanism. Potentiometric titrations showed that the modified activated carbon (ZrOx-AC) possesses positive charge at pH lower than 7, and FTIR analysis demonstrated that zirconium ions interact mainly with carboxylic groups on the activated carbon surfaces. Moreover, XPS analysis demonstrated that Zr(IV) interacts with oxalate ions, and the fluoride adsorption mechanism is likely to involve $–OH^-$ exchange from zirconyl oxalate complexes.

Keywords

adsorption; fluoride; zirconium; activated carbon; oxalic acid

Supporting information

Table S1–S5 and Figure S1–S8 are available free of charge via Internet at http://pubs.acs.org.

1. Introduction

Fluoride can be present in drinking water and it is considered beneficial at levels about 0.7 mg L^{-1}, but hazardous if it exceeds 1.5 mg L^{-1}, which is the limit recommended by the World Health Organization (WHO). Exposure to high fluoride concentrations often occurs through drinking groundwater, one of the main sources of potable water, and can result in fluorosis (dental and skeletal abnormalities) or neurological damage in severe cases [2]. Fluoride concentrations, up to 30 mg L^{-1} can be found in ground water in many parts of the globe, and it is present at least in 25 countries [1–3].

A number of papers have focused on engineered adsorbents for fluoride removal from aqueous solutions, and the sorbents include activated and impregnated alumina [4,5], clays, minerals and plants [6–8], activated carbon and nanotubes [9,10], rare oxides [11], polymeric materials and resins [12,13]. It is also know that the incorporation of some metal oxides like iron(III), manganese(II, IV), lanthanum(III), aluminum(III), zirconium(IV) or titanium(IV) into sorbent surfaces can significantly increase fluoride adsorption capacity [4,14–18]. Activated carbon, with native (unmodified) surfaces, is a poor sorbent for fluoride from water, but can provides a stable support for achieving high dispersion of metal phases that are powerful fluoride sorbents, and can also inhibit sintering or bulk precipitation of those active metal particles. When this carbonaceous material is impregnated with zirconium(IV) and its metal complexes, the adsorption capacity has been reported to improve by a factor of 3–5 [19]. The control over carbon surface area and the size distribution of the loaded metal phases are key factors to increase the fluoride adsorption capacity.

Some research has been focused in loading Zr(IV) into several adsorbents by impregnation or precipitation using base-initiated particle nucleation of metal salt solution [14,20–24]. While this synthesis is simple to carry out, it is difficult to understand and optimize due to the effects of pH, ionic strength, the presence of complexing agents, or others that are known to affect the aggregation and reorganization of Zr(IV) particles. In many cases, the sorbent specific area drops due to pore blockage by Zr-containing particles whose average sizes range from nanometers to micrometers, and are uncontrolled in the conventional synthesis. We believe the intentional use of complexing (or chelating) ligands that can bind to particle surfaces or nuclei during the synthesis, could be potentially useful to control the growth and final particle size distribution of the dispersed metal. Organic acids have demonstrated a positive effect on reduction of oxide nanoparticle size during the nucleation and aggregation stage [25,26]. This approach has not been systematically used to load Zr-containing nanoparticles onto carbonaceous surfaces such activated carbons, and thus, take advantage of the high mechanical strength, excellent permeability in flow-through systems and high surface of activated carbon for future use in defluoridation processes for drinking water systems.

The aim of this research is to improve the fluoride adsorption capacity of granular activated carbon by controlling the particle size of Zr(IV)-containing particles with oxalic acid as complexing ligand during the impregnation process, and to propose the possible fluoride adsorption mechanisms.

2. Materials and Methods

2.1. Adsorbents

Zirconium impregnated activated carbon was prepared according to an experimental design that considered the ratio Zr(IV)/organic capping agent (Zr/OA) to determine the conditions that produced an adsorbent with the highest fluoride adsorption capacity. 0.1 g of commercial activated carbon (AC, F400) was added to 10 mL of $ZrOClO_2{\cdot}8H_2O$ solutions from 0.01 to 15% of Zr^{4+} during two days. Subsequently, the impregnated carbon was mixed with 10 mL of 0.01–12.2% oxalic acid solution during 1 day, and then it was filtered, rinsed, and dried at 60°C during 12 h. The impregnated adsorbent thus obtained was designated as ZrOx-AC. An analogous procedure was followed adding F400 to $ZrOClO_2{\cdot}8H_2O$ solution, and the resultant material was denoted as Zr-AC. All the impregnation processes were performed at 25°C.

2.2. Batch adsorption experiments

A fluoride ion stock solution (100 mg L^{-1}) of NaF was prepared in deionized water, and the test solutions were made by subsequent dilution of the fluoride solution.

Samples of 0.1 g of modified or non-modified activated carbon were added to 30 mL of fluoride solution (0.1 to 60 mg L^{-1}) to conical-bottom polypropylene tubes. The solution's pH was adjusted daily to 7.0±0.25 using 0.1 N HCl or NaOH, and all the experiments were monitored until equilibrium was achieved. this took about 7 days. Each adsorption point was performed by duplicated, and the standard deviation was less of 5%.

The fluoride concentration was measured by an Orion potentiometer coupled with a fluoride ion selective electrode. 10 mL of a Total Ionic Strength Adjustment Buffer (TISAB II) were added to 10 mL of water sample (withdrawn from each experiment) and standards. All measurements were carried out at 25°C, and the adsorption capacity (q_e, mg g^{-1}) was calculated as follows:

$$q_e = \frac{V(C_o - C_e)}{w} \quad (1)$$

where V is the total solution volume, w is the mass of adsorbent, C_0 and C_e are the initial and final (or equilibrium) fluoride concentration respectively. The experimental adsorption data was fitted by the Langmuir and Freundlich isotherm models expressed as:

$$q_e = \frac{q_{\max} b C_e}{1 + b C_e} \quad (2)$$

$$q_e = K C_e^{\,n} \quad (3)$$

where q_{max} is the maximum adsorption capacity (mg g^{-1}) and b (L mg^{-1}) the Langmuir constant related to the adsorption energy or "affinity. On the other hand, K ($mg^{1-1/n}L^{1/n}$ g^{-1}) and n are Freundlich constants related to the sorption capacity and the adsorption intensity, respectively.

2.3. Adsorption kinetics and effect of co-existing anions

A 1000 mg L^{-1} of fluoride stock was prepared from NaF in deionized water, and dilutions were made from this solution. For kinetic experiments, 0.63 g of the adsorbent were placed in a rotating basket that was positioned in a 1 L reactor filled with 0.75 L of deionized water, at pH 7. The reactor was then placed in a water bath at 25°C, and the basket impeller that was connected to a motor was set a 470 min^{-1}. Once a certain stock volume was added to the reactor to set the initial fluoride concentration at 20 mg L^{-1}, the experiment began.

The effect of 1, 10 and 50 mg L^{-1} of a co-existing anion mixture (chloride, sulphate, nitrate, carbonate and phosphate: prepared from sodium reagents) was performed in batch reactors during fluoride adsorption at 25°C, with a fixed adsorbent dose of 3.33 g L^{-1} and an initial fluoride concentration of 20 mg L^{-1}. The solution pH was adjusted daily at pH 7 until equilibrium was achieved (this took about 7 days). Then, water samples were withdrawn to measure the residual concentration, as already described.

2.4. Materials characterization

The pore size and surface area of Zr-oxalate modified activated carbon were calculated from N_2 adsorption-desorption isotherms at 77 K (Micrometrics ASAP 2020). Surface area was estimated from the BET isotherms, and the pore size distribution was obtained by using the density functional theory (DFT).

FTIR analyses were performed to verify changes in vibrational frequencies in the functional groups with a Nicolet iS10 FT-IR spectrophotometer, using KBr pellets. The influence of atmospheric water and CO_2 was always subtracted. The spectra (32 scans) were recorder at a resolution 4 cm^{-1}.

XPS measurements were made in a SPECS spectrometer with a Phoibos 100 hemispherical analyzer. The base pressure in the UHV chamber was below 10^{-7} kPa. The X-ray radiation source was monochromatic Al K (1486.74 eV) at 100 W X-ray power and anode voltage of 14.00 kV. The photo-excited electrons were analyzed in constant pass energy mode, using pass energy of 50 eV for the survey spectra and 10 eV for the high-resolution core level spectra. For comparative purposes, all spectra are referenced to 284.5 eV corresponding to C 1s region. Casa XPS software was used for data processing. Core level curve fitting in different components was performed using a Shirley background and a standard least squares algorithm.

Potentiometric titrations were assessed to determine the surface charge distribution (pH_{PZC}) of each adsorbent with an automatic titrator (Mettler-Toledo T70). A sample of 0.1 g was dispersed in 50 mL of 0.1M of NaCl as background electrolyte. Titration was carried out by stepwise addition of 0.001 mL of 0.1N NaOH to the flask while the solution was stirred under N_2 atmosphere to exclude CO_2. After each addition of titrant, the system was allowed to equilibrate until a stable pH value was obtained. The pK_a distribution was obtained with the SAEIUS-pK-Dist©(1994) program.

The zirconium content in 40 mg of each adsorbent was determined by acid digestion with 20 mL of HNO_3:H_2SO_4 (5:1) solution, then, the mixture was digested by 1 h at 150°C in a

microwave advanced digestion system (Milestone, Ethos 1), where the remaining solution was diluted until 50 mL with deionized water and then analyzed by inductively coupled plasma-optical emission spectroscopy (ICP-OES) with a Varian 730-ES spectrophotometer.

The particle size and morphology of the anchored Zr(IV) particles were determined by scanning electron microscopy (SEM, FEI XL 30SFEG). The crystalline structure of Zr(IV) particles were determine by X-ray diffraction (XRD) patterns obtained with a step time of 10 s and 2θ of 0.02° with a XRD D8 Advanced-Bruker Axs (Cu Kα radiation λ =1.546Å). The modified Zr-carbon materials were crushed before SEM and XRD analysis.

3. Results and discussion

3.1 Effect of Zr/oxalic acid ratio on adsorption capacity

The measured adsorption capacity (q, mg g^{-1}) as a function of the Zr/OA ratio showed that the maximum q was obtained with Zr/OA= 1.05 (7% of each Zr(IV) and OA), as observed in Figure 1A and Table S1 of Supporting Information. When oxalic acid was added at high concentration (14.3%, Zr/OA= 0.52) the adsorption capacity decreased about 94%, whereas an increase in q was noticed a lower percentages (2<Zr/OA<3.5) with Zr/OA 6.11 and 2.10, respectively. The adsorption capacity was 0.75 and 2.04 mg g^{-1} when Zr and OA were in equal concentrations of 2 and 12%, respectively, but the organic acid by itself did not improve the adsorption capacity when Zr(IV) was at 0.01% (Zr/OA 0.001). When F400 was impregnated only with Zr(IV), the adsorption capacity was 62 % lower compared to the optimal ratio. The Pareto plot (Figure S1) demonstrated the effect of the production variables established in the modification methodology, where the bars represent the influence of the factor in the impregnation process. The concentration of oxalic acid (OA) and Zr(IV) was more significant ($p<0.05$) over the adsorption capacity when forming the Zr-oxalate complex in one step (LR): L denotes the interaction between OA and Zr, and R the opposite relation. The response surface data are shown in Supporting Information (Table S1).

3.1.1 Adsorption isotherms—Fluoride adsorption isotherms of the optimum modified and non-modified F400 (Zr/OA= 1.05) are presented in Figure 1C. The experimental data were reasonably fitted by both Langmuir and Freundlich models, based on the correlation coefficient (r^2), see Table S2 of Supporting Information. The low values for parameter b (<1) and n (<2) indicated a high fluoride affinity for the adsorbent. These models were used only to quantitatively describe the data and to compare the sorbent performance. Aside from the Langmuir q_{max} parameter, that can be interpreted as monolayer coverage.

From the adsorption isotherms, it was shown that q_{max} was 17.70 mg g^{-1} when OA was used as complexing agent. This could be due to a possible enhancement of the positive charge of Zr(IV) when was forming the zirconyl oxalate complexes with the OA. The unpaired electrons, located in the oxygen atoms of Zr-oxalate containing molecules, can attract the electronegativity of the metallic ion to make it more positive, which allow a better attraction for F^-. By contrast, q_{max} for Zr-AC was lower than that of F400, indicating that in absence of OA the complexation of Zr(IV) complexes could be occurring in agreement with a previous work from our research group for TiO_2-AC [27]. It can be seen from Table S2

that both ZrOx-AC and Zr-AC showed higher values of parameter *b*. This is an indication that in presence of Zr(IV) the modified carbonaceous materials have a higher trend to adsorbed fluoride from aqueous phase [28].

Without the presence of OA, the adsorption capacity of Zr-AC, at C_e= 40 mg L^{-1}, was 68% lower than ZrOx-AC. The maximum adsorption capacity for ZrOx-AC was 3 times higher than Zr-impregnated coconut shell carbon (1.75 mg g^{-1}), iron-impregnated granular ceramic (2 mg g^{-1}), Ca-impregnated nutshell carbons (2.3 mg g^{-1}) and aligned carbon nanotubes [30–33].

As shown in Table 1, F400 does not contain zirconium, but Zr-AC and ZrOx-AC have 0.16 and 0.77% of the metal, respectively. It was found that the oxalic acid carried out more Zr(IV) ions from the solution to form oxalate complexes [34], and this behavior could indicated that in the presence of OA an enhancement in Zr(IV) ions content makes more favorable the fluoride affinity in the adsorbent. This result agreed with the increase of fluoride adsorption capacity of ZrOx-AC compared to Zr-AC that does not contain the complexing agent (OA).

3.2. Kinetic studies and effect of co-existing ions

Adsorption kinetics were performed in order to evaluate the fluoride adsorption rate in ZrOx-AC, and the results are shown in Figure S2A of Supporting Information. The Zr-impregnated activated carbon removed 71% of the fluoride initial concentration in the first 15 min. The adsorption rate was considered fast [35, 36] because the initial fluoride concentration decreased around 90% in 1 h, and the equilibrium was reached in 50 min.

During the fluoride uptake the initial pH decreased during the first 40 min of analysis until pH 6.84, then this kept constant up to 80 min of staring the experiment. It is important to point out that the surface of Zr-containing particles anchored on AC may not be very high, and some patches of unmodified activated carbon could participate during the fluoride sorption as well. In the course of the fluoride adsorption process, some reactions could be achieved at the same time between the non-modified and Zr-oxalate complexes of ZrOx-AC surface. This comparison can be appreciated with the pH change of F400 during fluoride uptake (Figure S2B of Supporting Information) that behaves in similar way to ZrOx-AC. This behavior suggests a possible H^+ exchange from oxygenated F400 groups and/or from the Zr-oxalate complexes with the fluoride anions when the adsorption process was performed. Afterwards, the pH increased up to 6.93, which can be attributed to –OH released from the Zr-oxalate complexes.

The effect of co-existing anions such chloride, sulphate, nitrate, phosphate and carbonate, usually found in water, on ZrOx–AC fluoride adsorption capacity is shown in Figure S2C (see Supporting Information). Results showed a decreased of 44, 49 and 55% on the adsorption capacity when competing anions were presented in a mixture of 1, 10 or 50 mg L^{-1} of each anion, respectively. Although the fluoride adsorption capacity notably decreased, it can be observed that Zr-oxalate complexes have affinity for fluoride ions even at very high concentration (>10 mg L^{-1}) of co-existing anions.

3.3. Material Characterization

3.3.1 Physical properties—Table 1 shows that the surface area of F400 (926.83 m^2g^{-1}) decreased 6.5% when contains Zr-oxalate complexes, but without the presences of oxalic acid (Zr-AC) the surface area falls about 50%. The increase of macropore volume in modified F400 (ZrOx-AC and Zr-AC) can be attributed to partially blocked pores (>50 nm) that create more pores in the macropore range between aggregates. As discussed above, in presence of the capping agent (OA) this aggregation is inhibited. Moreover, a reduction of 16 and 60% of micro- and mesopore volume, respectively, was also observed when AC was doped with ZrOx. This suggests that some of Zr-oxalate particles are less than 2 nm in size.

3.3.2. Microscopy studies—The surface morphology of ZrOx-AC is shown in Figure S3A (see Supporting Information). The bright regions correspond to the Zr-containing particles, confirmed by EDS analyses (see Figure S3B and S3D); and from the microscopy scale it can be seen that the size of those particles loaded on the F400 surface was less than 10 nm when OA was added. On the other hand, the Zr(IV) particle size on Zr-AC was up to 100 nm (see Figure S3C). The presence of residual chloride was noticed in the Zr-containing particles due to the $ZrOCl_2$ used as a source of zirconium ions. Furthermore, Al (0.62%) and Si (0.13%) were found in the modified activated carbon due to the main components of the activated carbon, besides of C (76.3%) and O (6.4%) elements.

3.3.3. Spectroscopy evidence—Changes in the vibrational frequencies of Zr(IV) bonds with functional groups of F400 surface were studied in order to elucidate the interaction of the metal ion with the carbonaceous surface and the complexing agent.

The FTIR spectra of OA and those of ZrOx-AC before and after the adsorption of fluoride are shown in Figure S4 (Supporting Information). The spectra of F400 (Figure S4b) showed fewer peaks of weaker intensity around 1510 and 1164–968 cm^{-1} that indicate the vibration of C=O, C-O and –OH from carbonyl, lactones and phenolic groups, respectively. A band in 3423 cm^{-1} was associated with silanol groups (Si-OH) and adsorbed water. When F400 was impregnated with Zr(IV) the FTIR spectra showed 2 absorption bands in the region of 600–700 cm^{-1} that were attributed for Zr-O bond in coordinated complexes [37]. A weak vibration band in 1084 cm^{-1} was related to Z=O from zirconyl groups [38,39]. Furthermore, a broad band centered in 1495 cm^{-1} may be attributed to bidentate carbonates formed from the interaction between atmospheric CO_2 and O_2- Zr^{4+} pairs, as well a weak broad band in 471 cm^{-1} indicated that Zr(IV) can be found in a monoclinic and tetragonal phase of ZrO_2 [38]. ZrOx-AC showed a broad and sharper band of great intensity in 467 cm^{-1} that was associated with Zr-O (related to ZrO_2) and Zr=O. The broad peaks centered at 992 and 1506 cm^{-1} were assigned to Zr-O and Zr-OH bonds, respectively, while peaks around 880 and 1108 cm^{-1} were related to C-O-C and –OH bonds from the OA and Zr-oxalate complex, respectively. Bands at 1308 and 1348 cm^{-1} denoted a combination of Zr-O and Zr-OH vibration bonds [40, 41]. The peak at 3400 cm^{-1} was due to the stretching and bending modes of coordinated water and –OH bond from Zr-OH and the organic acid. A narrow band of big intensity at 1680 cm^{-1} indicated the presence of C=O groups. It is important to point out the presence of atmospheric CO_2, that ZrOx-AC could have adsorbed, related to peaks at 2328 and 2349 cm^{-1}.

The IR spectrum of OA (Figure S4a) showed peaks at 563, 715, 1010, 1364, 1668 and 3452 cm^{-1} that are attributed to normal vibration modes of the oxalic acid. The broad of these peaks may be due to absorbed water in the sample. There were similarities and shifts in absorption bands of OA and ZrOx-AC spectrums. The most important differences related to carboxylic groups ($\Delta = \Delta_{C=O}$-Δ_{C-OH}) are due to the symmetry of the carbon-oxygen bonds, and reflect Zr(IV) interaction with the organic complexing agent. The band shift between ZrOx-AC and OA were 12 and 98 cm^{-1}, respectively. These results indicated that Zr(IV) ions have more involvement with the acidic –OH than with the carboxylate group (COO^{-}) from OA to form Zr-oxalate complexes.

When fluoride was adsorbed (ZrOx-AC+F, spectra e), the peak related to –OH groups (3400 cm^{-1}) had a sharper form and low intensity than ZrOx-AC (spectra d). These imply that hydroxyl groups are involved in fluoride adsorption process. Furthermore, vibrational changes occurred between 400–500 cm^{-1} when F^{-} was adsorbed and could be due to the formation of fluoride complexes with Zr-O groups. A broad and intense band at 1046 cm^{-1} could be an overlapping of vibration of Zr-O, C-O and Zr-OH bonds due to the interaction with fluoride ions. It is important to notice an 'inverse' peak around 1680 cm^{-1} that could be due to the C=O stretching vibrations found in this range. Those vibrations are more intense in the *s*-polarized than in the *p*-polarized scans, and a *p:s* ratio was used to present the FTIR spectra [42].

3.3.4. X-ray diffraction studies—Powder X-ray diffraction was carried out in order to identified the polymorphic phases of ZrO_2 found in FTIR analysis when F400 was modified with Zr(IV) and OA. Figure S5 (Supporting Information) shows the XRD patterns for ZrOx-AC, where two peaks at 2θ angles of 26.58 and 43.1° correspond to monoclinic and 35–36.5° to tetragonal zirconia structures, respectively [43]. ZrO_2 has three polymorphic phases at ambient temperature: monoclinic, tetragonal and cubic. The monoclinic phase is described as a distorted fluorite structure with the Zr atoms in seven-fold coordination sites, while the cubic structure is an 8-coordinated zirconium ions face-centered cubic lattice where each oxygen ion is located in a 4-coordinated zirconium tetrahedron. The tetragonal structure can be derived by stretching the cubic one [44].

3.3.5. Surface charge and pK_a distribution—Proton binding curves obtained from potentiometric titrations in Figure 1B demonstrated that Zr(IV) shifted the point zero charge (pH_{PZC}) of F400 from 9.97 to 3.28, however, when the adsorbent contained OA to form the Zr-oxalate complexes, the pH_{PZC} increased to 11.18 (see Table 1). Activated carbon has high affinity for Zr(IV) ions, and when they are adsorbed on carbon surfaces, zirconium-based Lewis acid sites are generated [30,34]. The adsorption sites become basic with the addition of OA to form Zr-oxalate complexes, due to the unpaired electrons and the π-bond system of the oxygen atoms of the oxalate ligand. ZrOx-AC thus possesses positive charge at the pH of adsorption experiments (pH 7). These conditions are favorable for fluoride adsorption due to electrostatic attraction between the positively charged adsorbent and the anionic F^{-}. At pH greater than the pH_{PZC}, the adsorbent is negatively charged and disfavor the adsorption process.

The pK_a intensity and distribution of modified and non-modified F400 is presented in Figure S6A (see Supporting Information). It can be seen an increase of weak acidic groups in pKa~11 when Zr(IV) was anchored on the F400 surface. A reduction of carboxylic groups (4<pK_a<7) was noticed when Zr and its oxalate complexes were loaded on the carbon surfaces, while an increase of phenolic and C=O groups (9<pK_a<11) was appreciated. The results demonstrated that –COOH groups played an important role in zirconium ion anchoring.

Because Zr(IV) is considered a strongly acidic cation with pK_a values between −4 and 1 (in aqueous solution) [45], an increased in the surface acidity of F400 was noticed when Zr(IV) is loaded in the carbonaceous surface. This was confirmed by pK_a 2.66 and 2.92 in Zr-AC and ZrOx-AC, respectively, where the shift in the pK_a value could be due to the interaction between the metal ion and some of the oxygenated groups contained in the F400 surface. The pK_a positions and amount of groups are listed in Table S3 (see Supporting Information).

When fluoride ions were adsorbed on ZrOx-AC (see Figure S6B), the distribution and intensity of pK_a peaks changed due to the interaction of zirconyl complexes with F^-. A pK_a shift of 0.16 was observed in pK_a ~6 related to carboxylic groups (4<pK_a<7) when F^- was presented in ZrOx-AC+F, as well as a decreased in intensity and amount of the functional group (see Table S3 of Supporting Information). Moreover, a new peak can be noticed around pK_a 4.50 that could suggest a structural arrangement in the Zr-oxalate complex where a carboxylic group (from the OA) may arise again when fluoride was linked to the metal complex. The identification of fluoride in the Zr-oxalate complexes may be related to a pK_a peak around 8.35. The fluoride ions increase the basicity of the metal complex, due to the basic adsorption sites developed of the interaction between Zr(IV) and OA, with the addition of a strong Lewis base such F^-. It is important to notice the low intensities of pK_a peaks when fluoride was adsorbed, where concentrations of less than 0.004 meq g^{-1} were detected.

3.3.6. XPS analyses—XPS analyses were performed to find out the possible Zr(IV)/oxalic acid structure formed during the impregnation process and the way that fluoride interacts with the metallic complex. Figure S7 (see Supporting Information) shows the XPS full spectra referenced to C 1s level at 284.5 eV. It can be seen that the binding energy of Zr 3d region corresponding to Zr-AC and ZrOx-AC was 182.5 eV in good agreement with 182.3 eV for Zr^{+4} in ZrO_2 [46]. An important increase can be noticed in the binding energy up to 183.3 eV for zirconium in ZrOx-AC. This is in agreement with 183.6 eV in the $3d^{5/2}$ region for $Zr(OH)_4$. In addition, the binding energy of O 1s region showed an increase in the ZrOx-AC up to 532.5 eV compared to 531.5 eV for Zr-AC and ZrOx-AC+F samples. F 1s region was not detected in Figure S7 for ZrOx-AC+F. By contrast, Cl 2p is present in all samples with binding energies in the Cl 2p region of 198.5, 201 and 200 eV for Zr-AC, ZrOx-AC and ZrOx-AC+F, respectively. The binding energy in Cl $2p^{3/2}$ region of chloride salts has been reported at 198.6 eV [47], which is in agreement with Zr-AC. Binding energies in Cl $2p^{3/2}$ region clearly increased in ZrOx-AC and ZrOx-AC+F. These results suggest that OA plays an important role in the capture and surface interaction between C at Zr atoms.

Figure 2 shows the XPS spectra in the C 1s region referenced at 284.5 eV. It can be seen from deconvoluted peaks that Zr-AC (Figure 2A) and ZrOx-AC+F (Figure 2C) showed similar functional groups. Besides C=C peak at 284.4 eV that corresponded to sp^2 carbon bonding, all samples showed carbonyl (C=O) and carboxylic groups (COOH) at very similar binding energies at 286.2 and 289.5–290.0 eV, respectively. However, ZrOx-AC (Figure 2B) developed an additional peak at high binding energy, about 293.3 eV. Okpalugo et al. [48] attributed this peak to $\pi \rightarrow \pi^*$ transitions. It can also be attributed to C=C-O surface group formed by OA surface functionalization [49–51].

Figure S8 (see Supporting Information) shows the XPS spectra in the Zr 3d region. Zr-AC and ZrOx-AC+F spectras showed similar binding energy of 182.5 eV in the Zr 3d5/2 region in agreement with the formation of ZrO_2 [52]. In presence of OA, ZrOx-AC showed an enhancement in the binding energy up to 183.3 eV. This indicates a more positive surface charge around Zr atoms, probably by the interaction of hydroxyl groups from activated carbon surface and Zr(IV) ions to form $Zr(OH)_2Cl_2$. The high value of 183.3 eV for the binging energy in Zr 3d5/2 region is in agreement with that reported by Barr [46] for $Zr(OH)_4$. Also, a small peak about 180.6 eV was detected and attributed to the formation of Zr-Cl bonding in agreement with that reported for Zr-Br at 179.3 eV [53]. The shift to higher binding energies for Zr-Cl in comparison to Zr-Br is due to Cl having more electronegative than Br, and therefore, the binding energy corresponding to Zr-Cl must be higher than that of Zr-Br bond. The presences of chloride in the Zr-oxalate particles were corroborated by EDS analyses, as discussed in Section 3.3.2.

XPS spectra suggest that OA clearly influences the formation of different Zr-based groups on carbon surface in agreement with the different oxygenated functional groups detected from the deconvoluted peaks of C 1s region showed in Figure 2. This inference was confirmed from the changes in the atomic surface composition (At wt.), compiled in Table S4 of Supporting Information. Carbon surface composition are higher in Zr-AC and ZrOx-AC+F samples than in ZrOx-AC. Oxygen surface composition in ZrOx-AC showed a remarkable increase from about 7 to 14% in comparison of Zr-AC and ZrOx-AC+F. This was due to the high degree of functionalization promoted by OA. Concomitantly, the atomic ratios At-C/At-Zr and At-C/At-Cl in ZrOx-AC showed a remarkably decrease in comparison of ratios estimated for Zr-AC. This result indicated a remaining of Zr and Cl in ZrOx-AC by a stronger interaction with OA, probably due to a specific oxygenated surface groups such C=C-O, indicated in Figure 2.

3.4 Fluoride adsorption mechanism

The multiple spectroscopic techniques used here together with potentiometric titrations provided valuable information regarding the fluoride adsorption process in Zr-oxalic acid impregnated activated carbon (ZrOx-AC). The spectroscopy analyses identified the main functional groups involved in both the anchoring of Zr(IV) ions on the commercial activated carbon (F400) and in the fluoride uptake. Moreover, these analyses helped to identify the zirconyl fluoride species on the carbon surface.

Hence, with all the evidence shown in this study, a possible fluoride adsorption mechanism can be postulated (Figure 3). First, Zr(IV) species from the hydrolysis of $ZrOCl_2$ ($ZrOOH^+$

or $[Zr(OH)_{2+x}•(4\text{-}x)H_2O]_4^{(8-4x)+}$) [24] adsorb on AC by –COOH groups through electrostatic interactions to form C-O-Zr bonds. It is important to consider that Zr(IV) can form tetrahedric and octahedric polymeric structures [21,55]. Therefore, it is possible to propose a first interaction between the oxygen functionalities of activated carbon surface, see Figure 3A.

A second reaction occurred when oxalic agent was added to form the zirconyl oxalate complex, where Zr(IV) interacts with –OH from the oxalic acid. It is possible to form six Zr-oxalate structures and several other configurations like dodecahedric arrangements [29,54]. ZrO_2 forms as well and could produce a 7-coordinated polyhedral species [39]. To simplify such configurations, an interaction between Zr(IV) and OA can be suggested in Figure 3B.

The hydrolysis of $ZrOCl_2$ in aqueous solution produces structures of four Zr atoms in each tetramer complex that is arranged in a square, and each zirconium atom is coordinated by four bridging OH groups and H_2O molecules that tend to polymerize. The concentration of the polymeric species can reach a supersaturation level and crystal nuclei of hydrous zirconia are generated, forming then primary particles [55]. The last step occurs when the aggregation of the primary particles takes place, see Figure 4, and it is apparently controlled by the formation of the primary particles. The presence of oxalic acid in this step can avoid the aggregate growth due to steric effects and electrostatic repulsion between particles, which is in agreement with the particle size of Zr-complexes reported by microscopy studies. The particle surface of the small Zr-oxalate particles bonded on AC and polymeric or based Zr-oxalate complexes physical or locally attached in the carbonaceous surface contribute to the increase of fluoride adsorption capacity.

Finally, fluoride attack Zr(IV) ions in the metal complexes and its adsorption occur in the ZrOx-AC surface with –OH displacement from the Zr-oxalate complexes. A chemical rearrangement could be carried out to form –COOH groups in the OA and/or to form Zr-oxyfluoride species ($ZrOF_x$), see Figure 3C. It is important to point out that ZrO_2 can develop di-, tri-, tetra-, and pentafluoro zirconium species without the presence of a complexing agent such as oxalic acid [39].

In conclusion, it was shown that addition of oxalic acid during the Zr-doping of activated carbon increased the fluoride adsorption capacity by a factor of 3 over simple Zr-doped AC at an optimum Zr/OA ratio of 1.05. Our work suggests that the enhancement mechanism involves OA complexation with Zr ions, which controls the nucleation and limits the growth of ZrO_2 particles that reduce Zr dispersion in the conventional method. Suppressing particle growth increases the zirconium active surface area and leaves some highly active Zr in the form of OA molecular complexes associated with carbon surface sites. Finally, the proposed fluoride adsorption mechanisms were a hydroxyl exchange from the Zr-oxalate surface sites and fluoride interaction with the positive charge of zirconium ions in Zr=O groups.

Acknowledgments

This work was financially supported by grants from CONACYT-Ciencia Basica (SEP-CB-2008-01-105920) and the Superfund Research Program (Brown University). Litza H. Velazquez thanks the scholarship received from CONACYT (209008), and to Dulce Partida, Guillermo Vidriales, and Carmen Rocha for their technical support, as well to the national laboratory LANBAMA for its help with the samples analyzes. The authors thank Dr. Conchi

Ania from the Instituto Nacional del Carbon (Oviedo, Spain) for her assistances on XPS analyzes. Finally, the authors thank R. Jaramillo for her assistance in the english writing.

References

1. UNICEF. WaterFront, Fluoride in water: an overview. Vol. 13. Programme Division; 1999. p. 11-14.
2. Ozsvath DL. Fluoride and environmental health: a review. Rev Environ Sci Technol. 2009; 8:59–79.
3. Mohapatra M, Anand S, Misha BK, Giles, Dion E, Singh P. Review of fluoride removal from drinking water. J Environ Man. 2009; 91:67–77.
4. Tripathy SS, Raichur AM. Abatement of fluoride from water using manganese dioxide-coated activated alumina. J Haz Mat. 2008; 153:1043–1051.
5. Ku Y, Chiou HM. The adsorption of fluoride ion from aqueous solution by activated alumina. Water Air Soil Pollut. 2002; 133:349–360.
6. Srimurali M, Pragathi A, Karthikeyan J. A study on removal of fluorides from drinking water by adsorption on to low-cost materials. Environ Pollut. 1998; 99:285–289. [PubMed: 15093323]
7. Gopal K, Srivastava SB, Shukla S, Bersillon JL. Contaminants in drinking water and its mitigation using suitable adsorbents: an overview. J Environ Biol. 2004; 2:1–10.
8. Bower CA, Hatcher JT. Adsorption of fluoride from aqueous solution by soils and minerals. J Soil Sci. 1967; 3:151–154.
9. Abe I, Iwasaki S, Tokimoto T, Kawasaki N, Nakamura T, Tanada S. Adsorption of fluoride ion onto carbonaceous materials. J Colloid Interface Sci. 2004; 275:35–39. [PubMed: 15158376]
10. Li YH, Wang S, Zhang X, Wei J, Xu C, Luan Z, Wu D. Adsorption of fluoride from water by aligned carbon nanotubes. Mat Res Bull. 2003; 38:469–476.
11. Raichuir AM, Basu MJ. Adsorption of fluoride onto mixed rare earth oxides. Sep Purif Technol. 2001; 24:121–127.
12. Mahmood SJ, Taj F, Parveen F, Usmani TH, Azmat R, Uddin F. Arsenic, fluoride and nitrate in drinking water: the problem and its possible solution. Res J Eviron Sci. 2007; 1:179–184.
13. Krupadam RJ, Khan MS, Das S. Adsorption of fluoride from water by surface-functionalized polyurethane foam. Water Sci Technol IWA. 2010; 62.4:759–765.
14. Liao XP, Shi B. Adsorption of fluoride on zirconium(IV)-impregnated collagen fiber. Environ Sci Technol. 2005; 39:4628–4632. [PubMed: 16047802]
15. Li Z, Deng S, Zhang X, Zhou W, Huang J, Yu G. Removal of fluoride from water using titanium-based adsorbents. Front Environ Sci Eng China. 2010; 4:414–420.
16. Fang L, Ghimiere KN, Kuriyanna M, Inoue K, Makino K. Removal of fluoride using some lanthanum (III)-loaded adsorbents with different functional groups and polymer matrices. J Chem Technol Biotechnol. 2003; 78:1038–1047.
17. Chen N, Zhang Z, Feng C, Li M, Zhu D, Sugiura N. Studies on fluoride adsorption of iron-impregnated granular ceramics from aqueous solutions. Mat Chem Phys. 2011; 125:293–298.
18. Leyva Ramos R, Ovalle-Turrubiartes J, Sanchez-Castillo MA. Adsorption of fluoride from aqueous solution on aluminum-impregnated carbon. Carbon. 1999; 37:609–617.
19. Janardhana C, Nageswara Rao G, Sathish RS, Lakshman VS. Study on the defluoridation of drinking water by impregnation of metal ions in activated charcoal. Indian J Chem Technol. 2006; 13:414–416.
20. Schmidt GT, Vlasova N, Zuzaan D, Kersten M, Daus B. Adsorption mechanism of arsenate by zirconyl-functionalized activated carbon. J Coll Inter Sci. 2008; 317:228–234.
21. Biswas BK, Inoue J, Inoue K, Ghimire KN, Harada H, Ohto K, Kawakita H. Adsorptive removal of As(V) and As(III) from water by a Zr(IV)-loaded orange waste gel. J Haz Mat. 2008; 154:1066–1074.
22. Zheng YM, Lim SF, Chen JP. Preparation and characterization of zirconium-based magnetic sorbent for arsenate removal. J Coll Interf Sci. 2009; 338:22–29.

23. Sandoval R, Cooper AM, Aymar K, Jain A, Hristovsi K. Removal of arsenic and methylene blue from water by granular activated carbon media impregnated with zirconium dioxide nanoparticles. J Haz Mat. 2001; 193:296–303.
24. Sathish RS, Raju NSR, Raju GS, Rao N, Kumar KA, Janardhana C. Equilibrium and kinetic studies for fluoride adsorption from water on Zirconium impregnated coconut shell carbon. Sep Sci Technol. 2007; 42:769–788.
25. Pettibone JM, Cwiertny DM, Sherer M, Grassian VH. Adsorption of organic acids on TiO_2 nanoparticles: effects of pH, nanoparticle size, and particle aggregation. Langmuir. 2008; 24:6659–6667. [PubMed: 18537279]
26. Ketabi SA, Kazemi AS, Bagheri-Mohagheghi MM. The effect of complexing agent on the crystallization of ZnO nanoparticles. J Phys. 2011; 77:679–688.
27. Cordero T, Chovelon JM, Duchamp C, Ferronato C, Matos J. Surface nano-aggregation and photocatalytic activity of TiO_2 on H-type activated carbons. Appl Catal B: Environ. 2007; 73:227–235.
28. Matos J, Hofman M, Pietzrak R. Synergy effect in the photocatalytic degragation of methylene blue on a suspended mixture of TiO_2 and N-contianing carbons. Carbon. 2013; 54:460–471.
29. Cotton, FA.; Wilkinson, G. Advanced Inorganic Chemistry. 5. Wiley; USA: 1998.
30. Sathish RS, Sairam S, Raja VG, Rao GN, Janardhana C. Defluoridation of water using zirconium impregnated coconut fiber carbon. Sep Sci Technol. 2008; 43:3676–3694.
31. Chen N, Zhang Z, Feng C, Li M, Zhu D, Sugiura N. Studies on fluoride adsorption of iron-impregnated granular creamics from aqueous solution. Mat Chem Phys. 2011; 125:293–298.
32. Hernández-Montoya V, Ramirez-Montoya LA, Bonilla-Petriciolet A, Móntes-Morán MA. Optimizing the removal of fluoride from water using new carbons obtained by modification of nut shell wit calcium solution from egg shell. Biochem Eng J. 2012; 62:1–7.
33. Li YH, Wang S, Zhang X, Wei J, Xu C, Wu D. Adsorption of fluoride from water by aligned carbon nanotubes. Mat Res Bull. 2003; 38:469–476.
34. Venable, FP. The chemical catalog company. Zirconium and its compounds. American Chemical Society; New York: USA: 1922.
35. Vitela-Rodriguez AV, Rangel-Mendez JR. Arsenic removal by modified activated carbon with iron hydro(oxide) nanoparticles. J Environ Manag. 2013; 114:225–231.
36. Swain SK, Patnaik T, Singh VK, Jha U, Patel RK, Dey RK. Kinetics, equilibrium and thermodynamic aspects of removal of fluoride from drinking water using meso-structured zirconium phosphate. Chem Eng J. 2011; 171:1218–1226.
37. Socrates, G. Infrared and Raman Characteristic group frequencies. Tables and Charts. 3. Wiley; USA: 2001.
38. Guo GY, Chen YL. New Zirconium Hydroxide. J Mater Sci. 2004; 39:4039–4043.
39. Chitrakar R, Tezuka S, Sooda A, Sakane K, Ooi K, Hirotsu T. Selective adsorption of phosphate from seawater and wastewater by amorphous zirconium hydroxide. J Coll Inter Sci. 2006; 97:426–433.
40. Duo X, Mohan D, Pittman CU, Yang S. Remediating fluoride form water using zirconium oxide. Chem Eng J. 2012; 198:236–245.
41. Jere GV, Santhamma MT. IR and laser Raman Studies on peroxo fluoro species of zirconium. Inorg Chim Acta. 1977; 24:57–61.
42. Hansen DM, Albaugh CE, Moran PD, Kuech TF. Chemical investigations of Ga As wafer bonded interfaces. J Appl Phys. 2001; 90:5991–5999.
43. Hristovsi KD, Westerhoff PK, Crittenden JC, Olson LW. Arsenate removal by nanostructured ZrO_2 spheres. Environ Sci Technol. 2008; 42:3786–3790. [PubMed: 18546723]
44. Qunbo F, Fuchi W, Huiling Z, Feng Z. Study of ZrO_2 phase structure and electronic properties. Molecular Simulation. 2008; 34:1099–1103.
45. Wulfsberg, G. Inorganic Chemistry. University Science Books; U.S.A: 2000.
46. Barr TL. An ESCA study of termination of the passivation of elemental metals. J Phys Chem. 1978; 82:1801–1810.

47. Dillard JD, Taylor LT, Seals RD, Alexander R. Core electron binding energy study of Group IIb-VIIa compounds. Inor Chem. 1973; 12:2485–2487.

48. Okpalugo TIT, Papakonstantinou P, Murphy H, McLaughlin J, Brown NMD. High resolution XPS characterization of chemical functionalized MWCNTs and SWCNTs. Carbon. 2005; 43:153–161.

49. Balazs DJ, Triandafillu K, Chevolot Y, Aronsson BO, Harms H, Descouts P, Mathieu HJ. Surface Modification of PVC endotracheal tubes by oxygen discharge to reduce bacterial adhesion. Surf Inter Anal. 2003; 35:301–309.

50. Lee WH, Kim SJ, Lee WJ, Lee JG, Haddon RC, Reucroft PJ. X-ray photoelectron spectroscopy studies of surface modified single-walled carbon nanotube materials. Appl Surf Sci. 2001; 181:121–7.

51. Martinez MT, Callejas MA, Benito AM, Cochet M, Seeger S, Anson A, Schreiber J. Sensitivity of single wall carbon nanotubes to oxidative processing: structural modification, intercalation and functionalization. Carbon. 2003; 41:2247–2256.

52. Liu B, Hu J, Ford JS. Electrochemical deposition of zirconia films on diamond electrodes. Electrochem Solid-State Lett. 2011; 14:D20–D22.

53. Ebert H, Knecht M, Muhler M, Helmer O, Bensch W. Experimental and theoretical band structure of the layer compound ZrSiTe. J Phys Chem. 1995; 99:3326–3330.

54. Yang JY, Fu YL, Ren JL, Ng SW. Calcium dipotassium tetraoxalatozirconate (IV) octahydrate. Acta Crystall Section E. 2006; 62:2424–2426.

55. Koji M, Ohgai M. Formation mechanism of hydrous zirconia particles produced by the hydrolysis of $ZrOCl_2$ solutions: III, kinetics study for the nucleation and crystal-growth processes of primary particles. J Am Ceram Soc. 2001; 84:2303–2312.

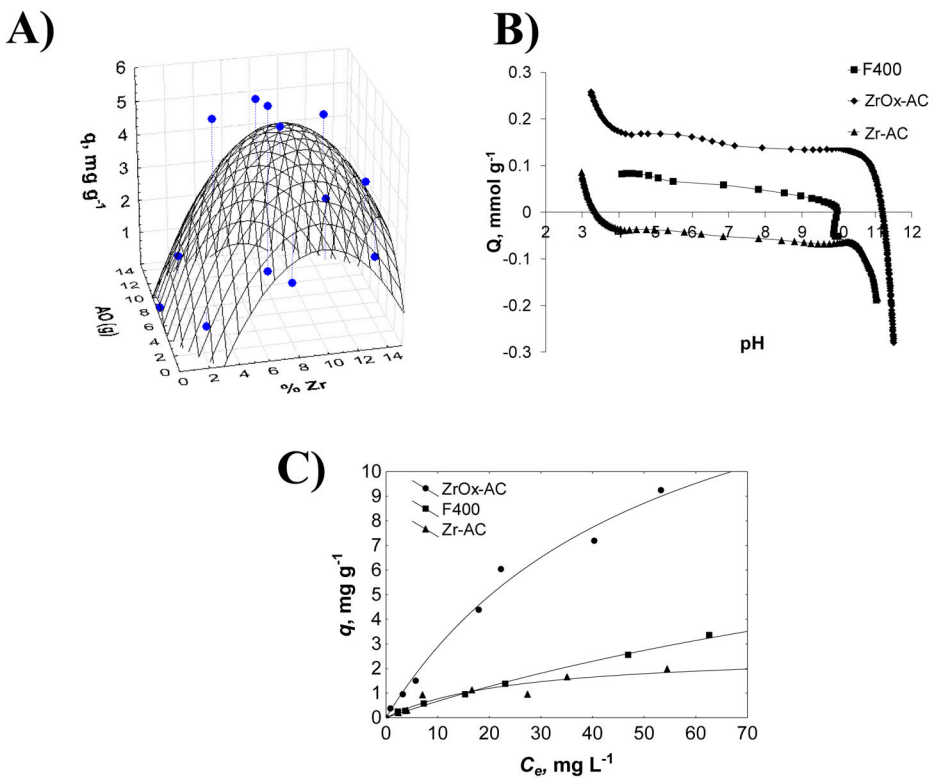

Figure 1.

A) Response surface of fluoride adsorption capacity as a function of percentage of Zr(IV), B) Surface charge distribution of F400, Zr-AC and ZrOx-AC in 0.01 N NaCl and, C) Fluoride adsorption isotherms of modified and non-modified F400, at pH 7 and 25°C, where the solid lines indicate the Langmuir model.

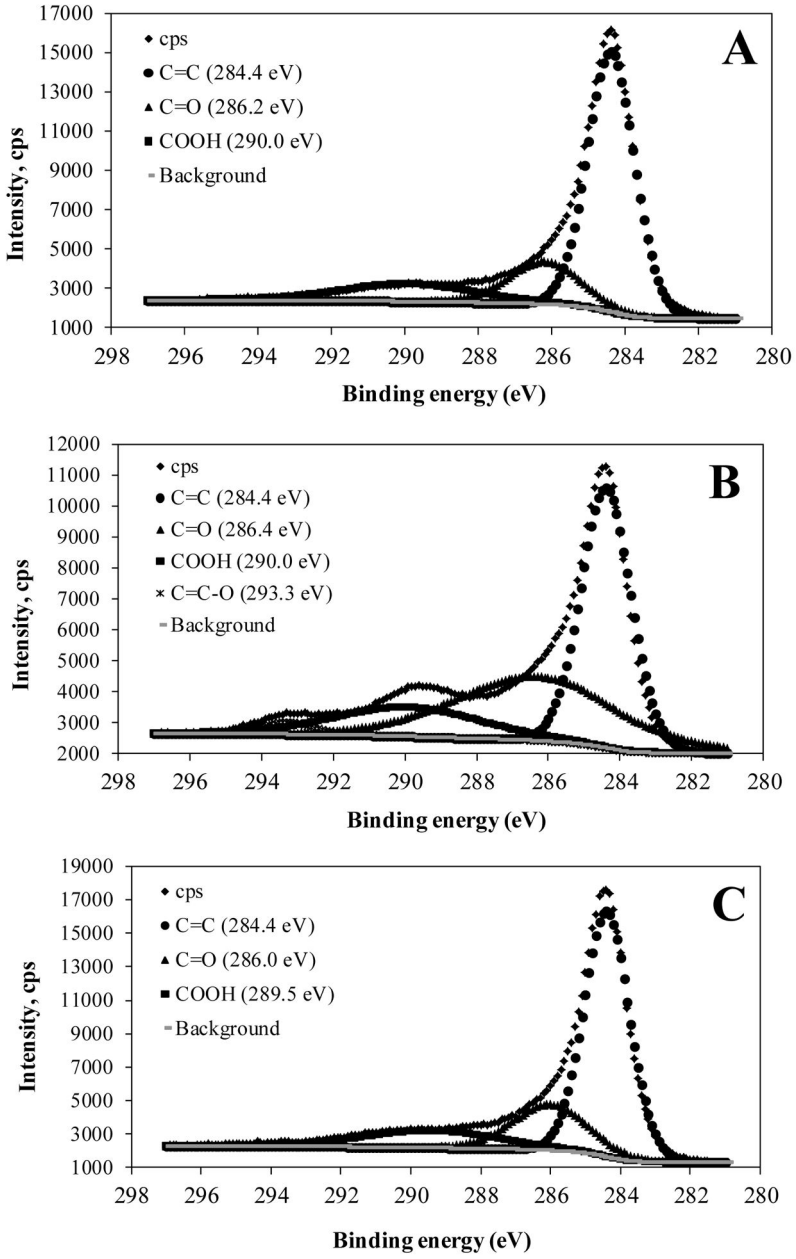

Figure 2.

XPS spectra in the C 1s region referenced at 284.5 eV for: A) Zr-AC, B) ZrOx-AC, and C) ZrOx-AC+F.

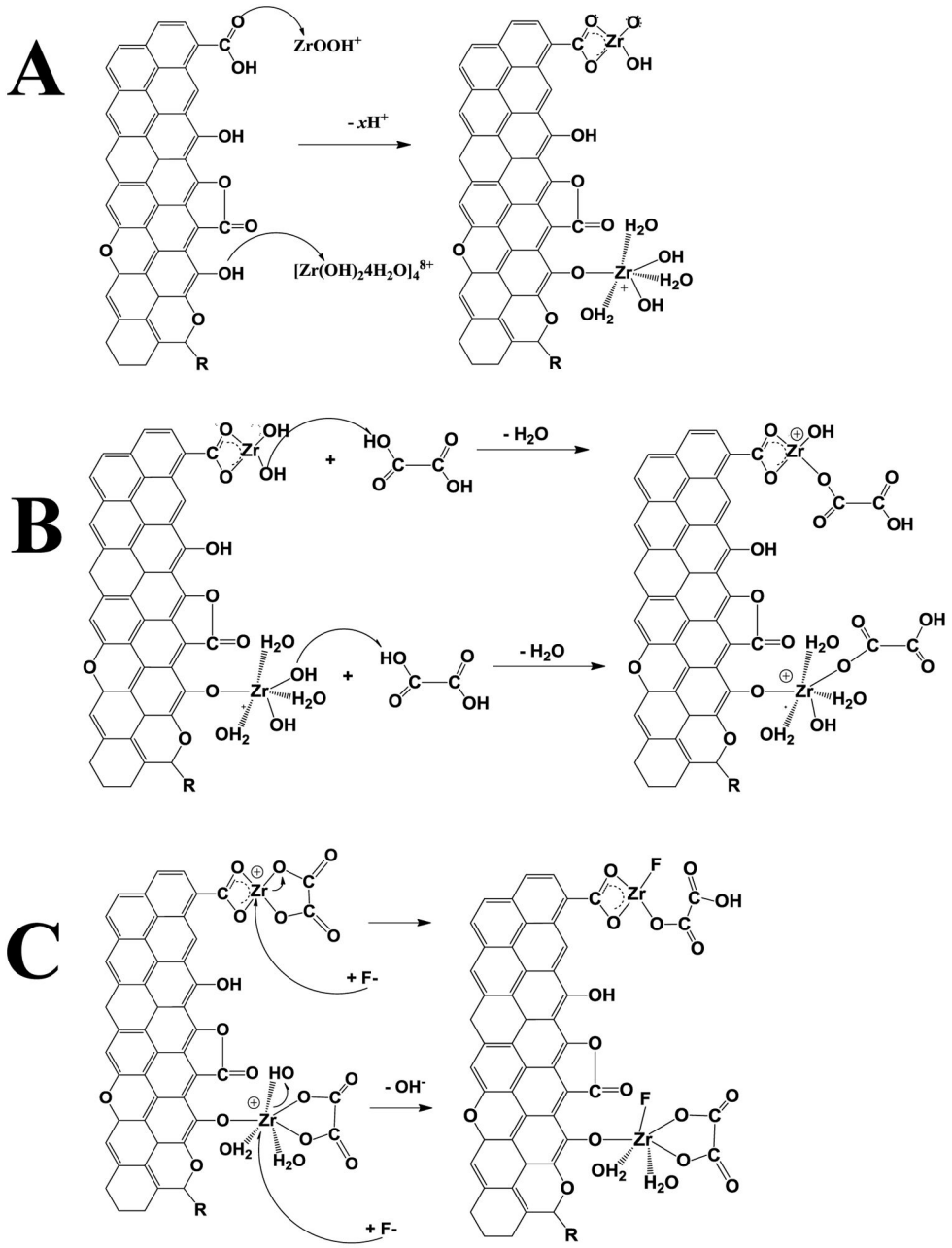

Figure 3.
Possible fluoride adsorption mechanism.

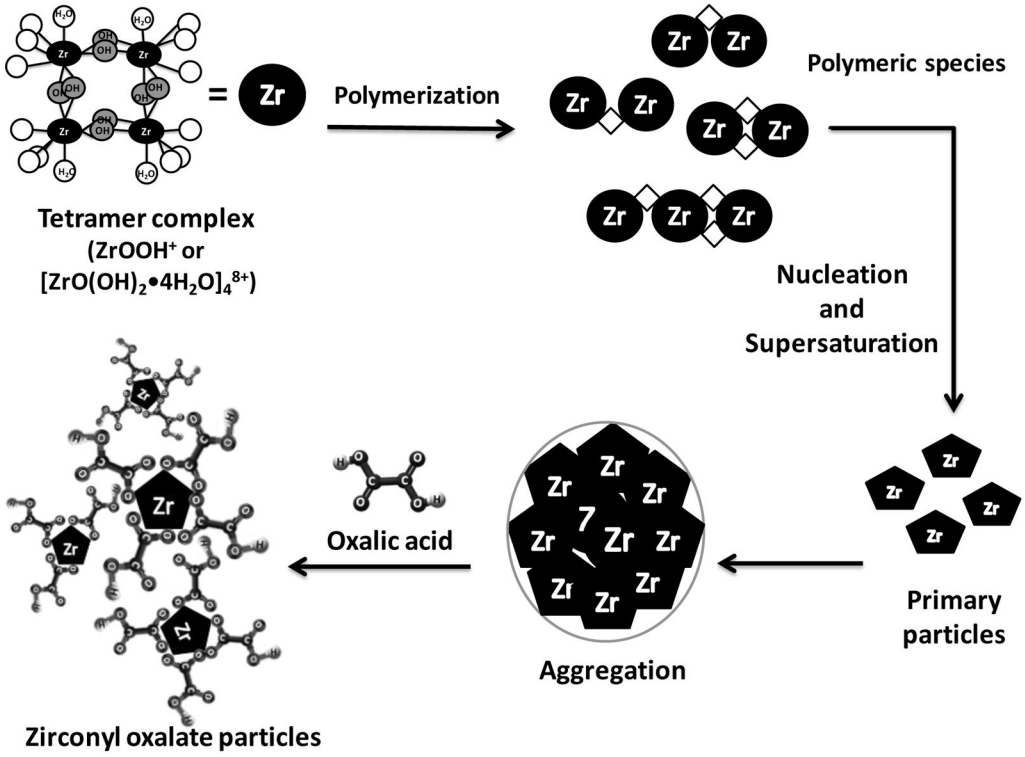

Figure 4.

Scheme of hydrous zirconia formation by hydrolysis of $ZrOCl_2$ solution, its polymerization and the interaction of Zr with oxalic acid to form Zr-oxalate complexes. ◇ represents –ol bridge. Adapted from [54].

Table 1

Physicochemical characterization of modified and non-modified activated carbon F400.

Sample	BET (m^2 g^{-1})	Pore volume (cm^3 g^{-1})			pH_{PZC}	Zr%	q^*, mg g^{-1}
		Micropore (<2 nm)	Mesopore (2–50 nm)	Macropore (>50 nm)			
F400	927	0.330	0.074	0.003	9.97	ND	2.25
Zr-AC	546	0.174	0.030	0.004	3.28	0.16	1.85
† ZrOx-AC	867	0.278	0.029	0.025	11.18	0.77	7.40

ND= non determined.

*Adsorption capacity at C_e= 40 mg L^{-1}, pH 7 and 25°C.

†The Zr/OA ratio was 1.05.